

Validation report of reprocessed IASI L2 CO CDR for Metop-A and B

Validated products:

Identifier	Name	Acronym
O3M-517.A	IASI A CO CDR (Climate Data Record)	MxI-DR1-CO
O3M-517.B	IASI B CO CDR (Climate Data Record)	MxI-DR1-CO

Authors:

Name	Institute
Bavo Langerock	Royal Belgian Institute for Space Aeronomy

Reporting period: July 2007 – December 2021

Input data versions: IASI/Metop CDR EumetSAT reprocessed CO and SO2 netCDF

Data processor versions: Forli v20151001_sp20171122

authors B. Langerock

reference AF/AC/IASI/VR/IASI_CO_CDR_L2

document type AC-SAF Validation Report

issue 1

revision 1

date of issue 30 November 2023

products

product version Forli v20151001_sp20171122

distribution

Function	Organisation
AC-SAF	EUMETSAT, BIRA-IASB, DLR, DMI, DWD, FMI, HNMS/AUTH, KNMI, RMI

external contributors

NDACC teams contributing ground-based correlative measurements

PI	Organisation	Acronym	Country
De Maziere, M.	Royal Belgian Institute for Space Aeronomy	BIRA.IASB	BELGIUM
Mellqvist, J.	Chalmers University of Technology	CTH	SWEDEN
Notholt, J.	Institut fuer Umweltphysik, Universitaet Bremen	IUP	GERMANY
Blumenstock, T.	Karlsruhe Institute of Technology	KIT	GERMANY
Schneider, M.	Karlsruhe Institute of Technology	KIT	GERMANY
Sussmann, R.	Karlsruhe Institute of Technology - Institute for Meteorology and Climate Research - Atmospheric Environmental Research	KIT.IMK.IFU	GERMANY
Hannigan, J.	National Center for Atmospheric Research	NCAR	UNITED STATES
Smale, D.	National Institute of Water and Atmospheric Research	NIWA	NEW ZEALAND
Makarova, M.	Saint Petersburg State University	SPBU	RUSSIAN FEDERATION
Mahieu, E.	University of Liege	ULG	BELGIUM
Nagahama, T.	University of Nagoya	UNAGOYA	JAPAN
Grutter, M.	Universidad Nacional Autonoma de Mexico	UNAM	MEXICO
Jones, N.	University of Wollongong	UOW	AUSTRALIA

document change record

Issue	Rev.	Date	Section	Description of Change
1	0	31.10.2022	-	Version submitted for review
1	1	30.11.2023		Revision with reviewer recommendations

AC SAF product ID numbers

AC SAF internal identifier	Description
IASI CDR CO	O3M-517.A, O3M-517.B

Validation report of reprocessed IASI L2 CO CDR for Metop-A and B

CONTENTS

ACRONYMS AND ABBREVIATIONS	4
1. INTRODUCTION.....	6
1.1. Scope of this document.....	6
2. VALIDATION WITH NDACC GROUND-BASED FTIR CO DATA	7
2.1. Measurement characterisation	8
2.2. Comparison methodology.....	11
2.3. Comparison statistics.....	13
2.4. Long term stability of comparison results	17
3. DISCUSSION AND CONCLUSIONS	24
4. REFERENCES.....	26
4.1. Applicable documents	26
4.2. Reference documents.....	26

ACRONYMS AND ABBREVIATIONS

AVK	Averaging kernel
AC SAF	Atmospheric Composition Monitoring Satellite Application Facility CDOP-3: Third Continuous Development and Operations Phase
CDR	Climate Data Record
ESA	European Space Agency
EUMETSAT	European Organisation for the Exploitation of Meteorological Satellites
FORLI	Fast Optimal Retrievals on Layers for IASI
GB	GroundBased
IASI	Infrared Atmospheric Sounding Interferometer
NDACC IRWG	NDACC Infrared Working Group
LOS	Line Of Sight
NDACC	Network for the Detection of Atmospheric Composition Change
O3M-SAF	Ozone and Atmospheric Chemistry Monitoring Satellite Application Facility
PC	Partial Column
SNR	Signal to Noise Ratio
SZA	Solar Zenith Angle
TOA	Top Of the Atmosphere
VCD	Vertical Column Density
VMR	Volume Mixing Ratio
WMO	World Meteorological Organization

Introduction to EUMETSAT Satellite Application Facility on Atmospheric Composition monitoring (AC SAF)

Background

The monitoring of atmospheric chemistry is essential due to several human caused changes in the atmosphere, like global warming, loss of stratospheric ozone, increasing UV radiation, and pollution. Furthermore, the monitoring is used to react to the threats caused by the natural hazards as well as follow the effects of the international protocols.

Therefore, monitoring the chemical composition and radiation of the atmosphere is a very important duty for EUMETSAT and the target is to provide information for policy makers, scientists and general public.

Objectives

The main objectives of the AC SAF is to process, archive, validate and disseminate atmospheric composition products (O₃, NO₂, SO₂, BrO, HCHO, H₂O, OCIO, CO, NH₃), aerosol products and surface ultraviolet radiation products utilising the satellites of EUMETSAT. The majority of the AC SAF products are based on data from the GOME-2 and IASI instruments onboard Metop satellites.

Another important task besides the near real-time (NRT) and offline data dissemination is the provision of long-term, high-quality atmospheric composition products resulting from reprocessing activities.

Product categories, timeliness and dissemination

NRT products are available in less than three hours after measurement. These products are disseminated via EUMETCast, WMO GTS or internet.

- Near real-time trace gas columns (total and tropospheric O₃ and NO₂, total SO₂, total HCHO, CO) and high-resolution ozone profiles
- Near real-time absorbing aerosol indexes from main science channels and polarization measurement detectors
- Near real-time UV indexes, clear-sky and cloud-corrected

Offline products are available within two weeks after measurement and disseminated via dedicated web services at EUMETSAT and AC SAF.

- Offline trace gas columns (total and tropospheric O₃ and NO₂, total SO₂, total BrO, total HCHO, total H₂O) and high-resolution ozone profiles
- Offline absorbing aerosol indexes from main science channels and polarization measurement detectors
- Offline surface UV, daily doses and daily maximum values with several weighting functions

Data records are available after reprocessing activities from the EUMETSAT Data Centre and/or the AC SAF archives.

- Data records generated in reprocessing
- Lambertian-equivalent reflectivity
- Total OCIO

Users can access the AC SAF offline products and data records (free of charge) by registering at the AC SAF web site.

More information about the AC SAF project, products and services: <https://acsaf.org/>

AC SAF Helpdesk: helpdesk@acsaf.org

Twitter: https://twitter.com/Atmospheric_SAF

1. INTRODUCTION

1.1. Scope of this document

The present document reports on the verification and validation of Metop-A and B reprocessed CO data over the July 2007 – Dec. 2021 time period for Metop-A and Feb. 2013 – Dec 2021 time period for Metop-B. These Climate data records (CDR) were produced with the FORLI v20151001 Data Processor operated at EUMETSAT. This report includes verification work performed using ground-based carbon monoxide profile measurements from the NDACC network. The aim is to investigate whether the IASI CO CDR product fulfils the product requirements in terms of accuracy (Threshold accuracy: 25%; Target accuracy: 12%; Optimal: 5%), as stated in the FORLI-CO product specification, requirement and assessment document [AD1] and in the Product Requirements Document [AD2]. For high pollution or low signal situations, the target value is 20% and the optimal value is 10%.

NDACC FTIR instruments measure direct sunlight and this document therefore only reports on the daytime IASI CO data. An evaluation of nighttime pixels can be found in the IASI CO L3 validation report [VRL3].

2. VALIDATION WITH NDACC GROUND-BASED FTIR CO DATA

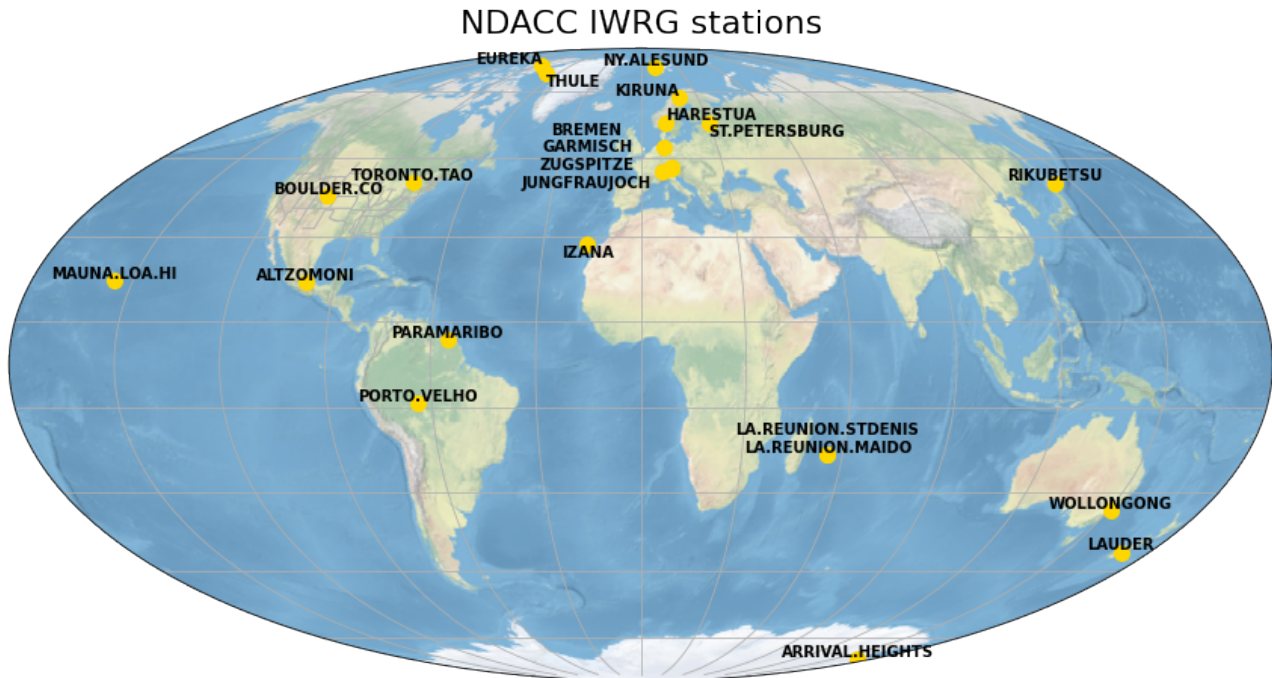


Figure 2.1 Overview of the 23 NDACC IRWG stations that contributed with CO measurement data.

This chapter describes in detail the comparison between the IASI CO CDR against FTIR measurement data publicly available from the NDACC (Network for the Detection of Atmospheric Composition Change) database. All available NDACC data covering July 2007 - 2021 is used. Twenty-three NDACC sites provide CO data during this period (Figure 2.1, Figure 2.2 and Figure 2.3).

Sections 2.1 and 2.2 describe the main characteristics of the measurements used in the comparison and the comparison methodology respectively. The comparison methodology follows closely the setup used in the validation report for the NRT CO product [VR1] with the main difference that here the groundbased prior is used as the common prior in the comparisons..

2.1. Measurement characterisation

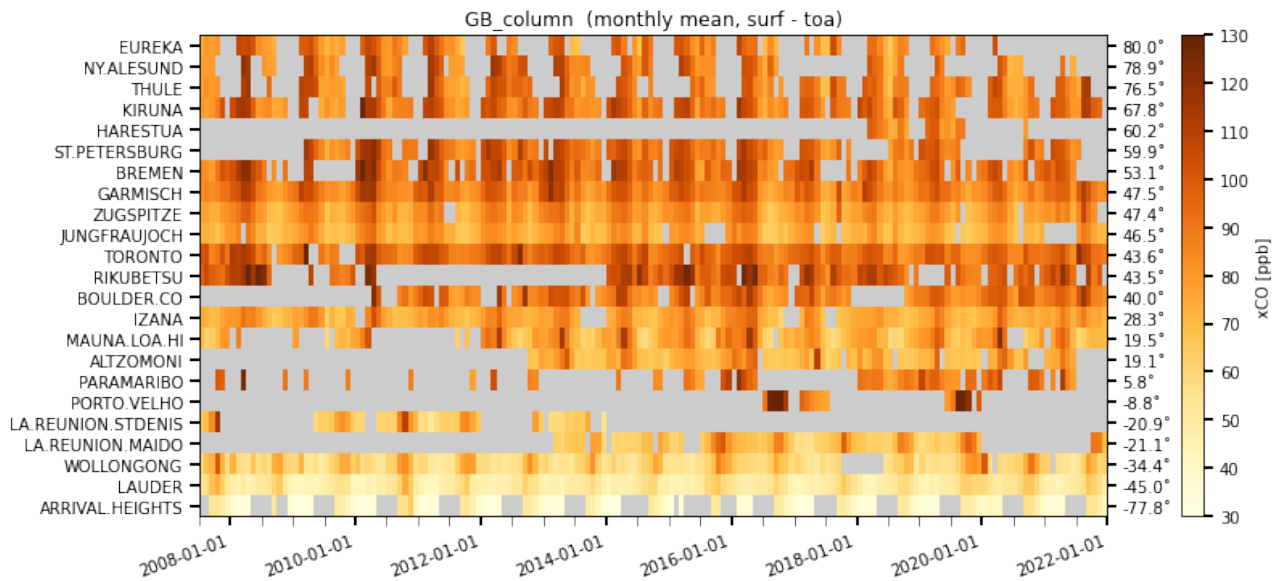


Figure 2.2 Overview of NDACC instruments with CO measurement data since mid 2007. Time series shows xCO. Sites are sorted by latitude which is indicated on the right. FTIR measures direct sunlight and hence no measurements are available at high latitude stations during local winter.

NDACC FTIR

NDACC FTIR CO measurements are sensitive to the troposphere and stratosphere between the surface and approximately 30km. NDACC CO data is formatted in GEOMS hdf files which contain the retrieved CO VMR profiles between the surface and the top of the atmosphere (TOA), the associated averaging kernels and *a-priori* profiles. An example FTIR averaging kernel is shown in Figure 2.7 including the sensitivity curve. The *a-priori* profiles are obtained from the Whole Atmosphere Community Climate Model (WACCM) model.

The typical total column uncertainty on the FTIR CO data is estimated at 4% for the systematic uncertainty¹ and 3% for the random uncertainty. The systematic uncertainty is dominated by the spectroscopic uncertainty. Figure 2.2 provides an overview of all NDACC CO data for the mentioned time period as dry-air averaged columns. All FTIR spectrometers are Bruker type spectrometers, except the instrument at Toronto which is a Bomem spectrometer. For further details on the instruments, we refer to Vigouroux *et al.* (2007 and 2020). Typical values for the FTIR degrees of freedom (DOF) range between two and three.

IASI FORLI

Similar as NDACC FTIR profiles, IASI FORLI CO profiles are obtained by optimal estimation (Rodgers 2000, Hurtmans *et al.* 2012) and the associated averaging kernels and *a-priori* profiles are distributed in netCDF files (see [PUM]). The quality filter proposed in the PUM is applied and only pixels with $co_qflag \geq 2$ (best quality pixels) are taken into account. In addition, pixels with negative surface pressure or with $flag_dayunit$ equal to 1 are removed from the comparisons. Pixels with total co column ($co_integrated$) above 0.5 mol/m^2 are also removed from the comparisons. A single IASI *a-priori* profile is used in the retrieval and is derived from tropospheric profiles from the LMDz-INCA chemistry transport model (from the ground up to 15.6 km), from UTLS profiles obtained from ACE-FTS profiles and from MOZAIC aircraft profiles, Hurtmans *et al.* (2012), George *et al.* (2015).

¹ Systematic and random uncertainty are interpreted as estimates for respectively the accuracy and precision of the measurements. Random uncertainties are lowered with the \sqrt{N} rule when averaging N measurements in time.

Figure 2.3 shows the IASI-A xCO columns at the different NDACC sites (see colocation criteria in Section 2.2). The difference between the IASI retrieved and *a priori* columns is shown in Figure 2.4. The IASI prior is systematically overestimating the retrieved columns in the southern hemisphere and this will be taken into account in the next section that describes the chosen comparison methodology.

According to [AD1] the uncertainties on the IASI profiles are obtained from the retrieval covariance matrix (Rodgers 2000). This contains an estimate of the smoothing uncertainty and the spectral noise (being relatively small to the smoothing contribution). Overall uncertainties are ranging from 5% to 15% at high latitudes (George *et al.* 2015). The uncertainty estimate does not contain model parameter errors such as spectroscopic parameters. The higher uncertainty at the high latitude sites is dominated by the smoothing error and is related to reduced sensitivity in the retrieval.

The IASI DOFS reached at the NDACC sites are shown in Figure 2.5 and are typically above 1 and can reach values above 1.5 depending on the geographical location and seasons (summer season has typically higher DOFS).

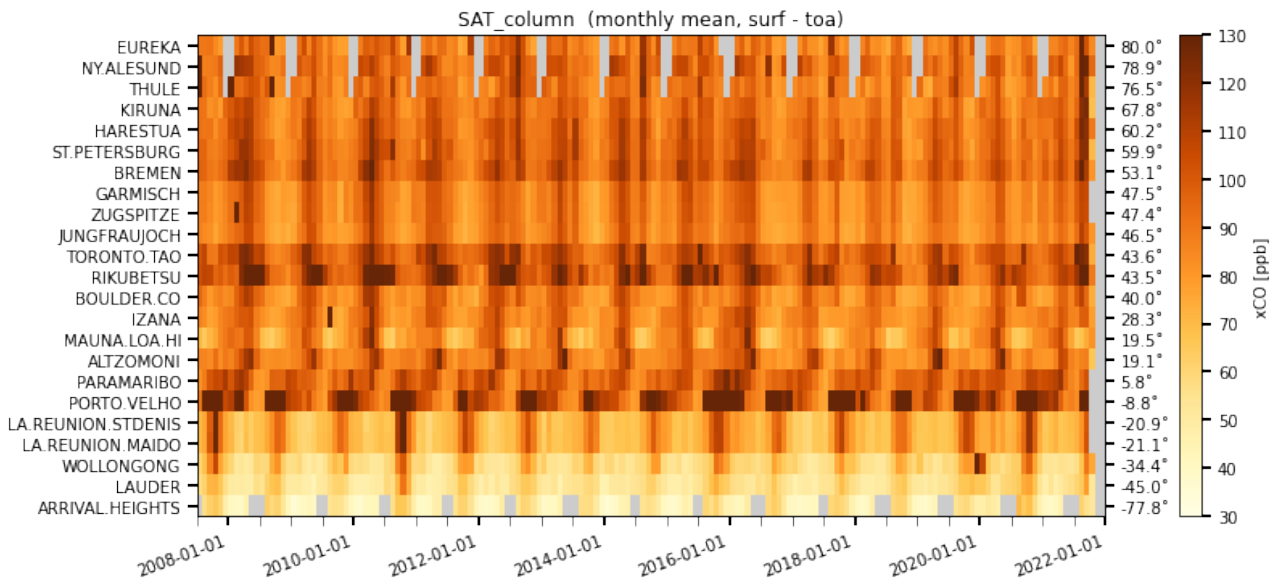


Figure 2.3 Mosaic of IASI A xCO at the different NDACC sites for the period 2007-2021. Similar to Figure 2.2, sites are sorted according to latitude.

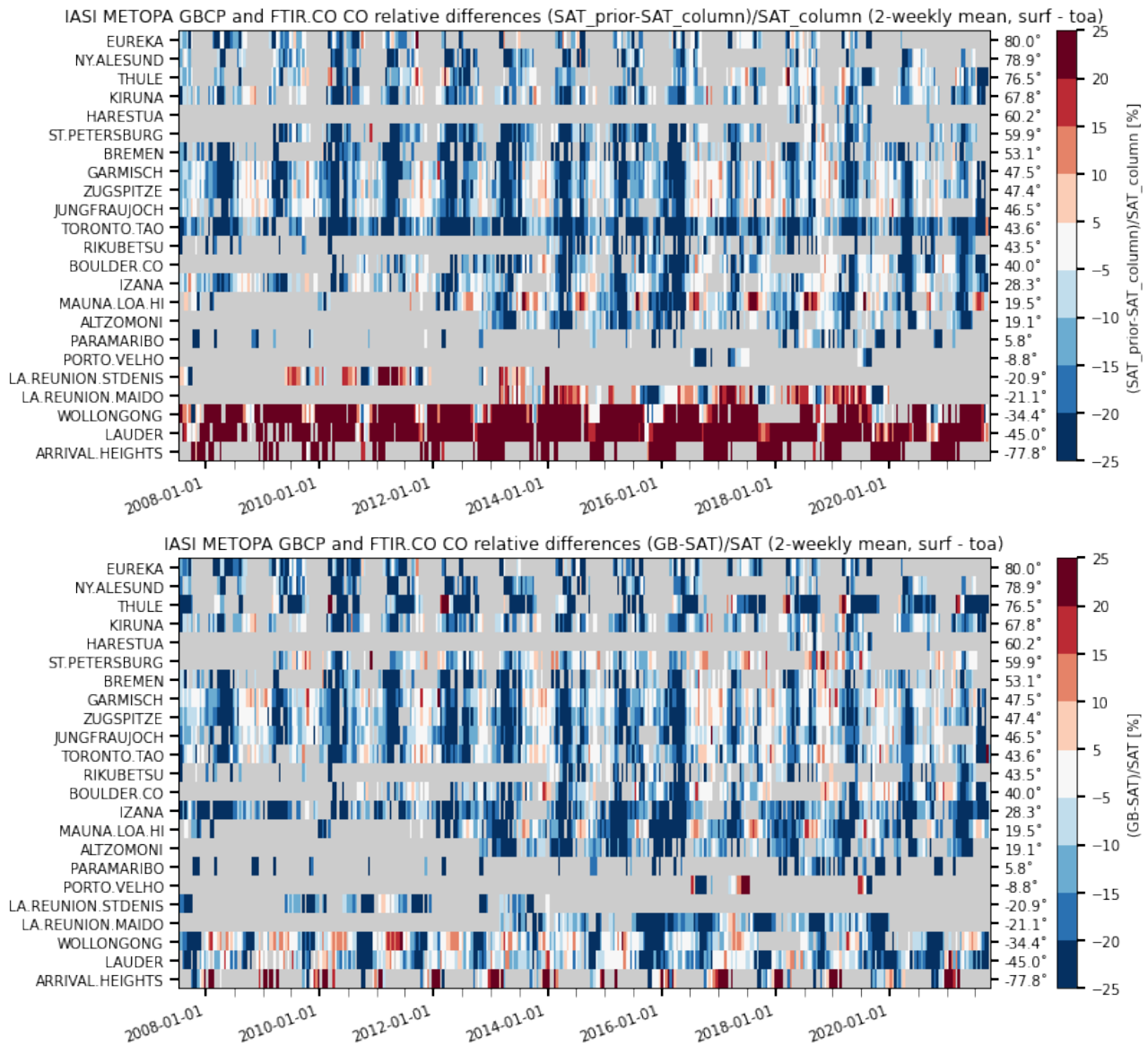


Figure 2.4 Mosaic of IASI-A CO relative differences between IASI retrieved and *a priori* columns at the different NDACC sites (top) and the difference between the IASI retrieved and the GB prior. Similar to Figure 2.2, sites are sorted according to latitude. The IASI prior is overestimating the retrieved columns in the southern hemisphere while the GB prior is closer to the true state. For Toronto the IASI prior is too low.

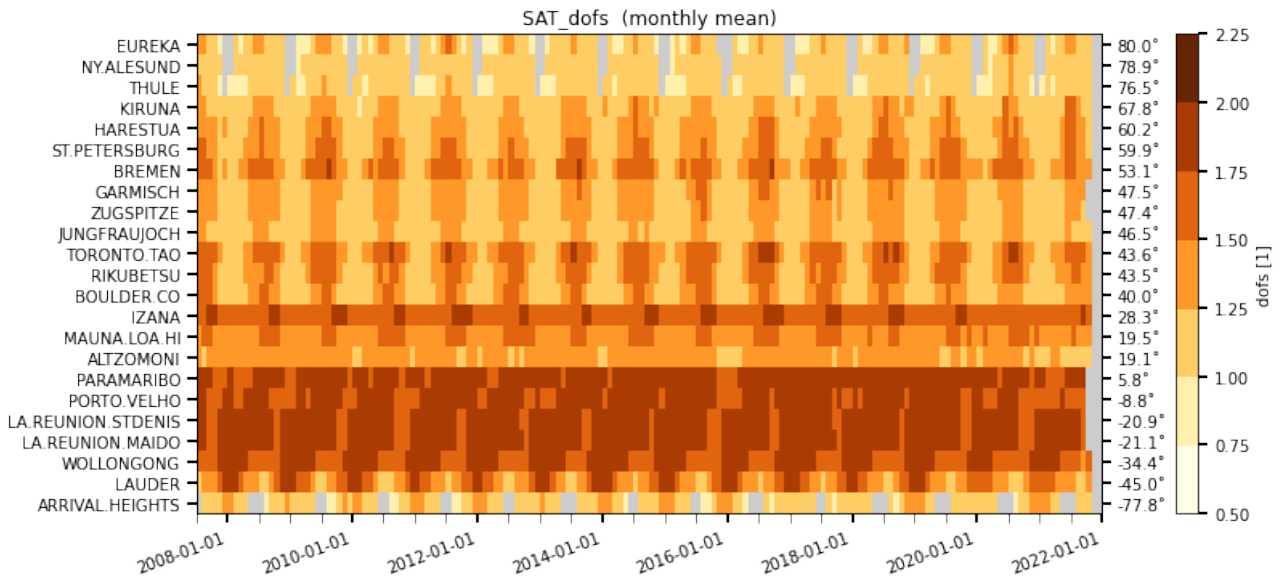


Figure 2.5 Mosaic of IASI-A CO degrees of freedom (DOF) at the different NDACC sites for the period mid 2007-2021. Similar to Figure 2.2, sites are sorted according to latitude. At the high latitude sites a lower DOF is observed during local spring months.

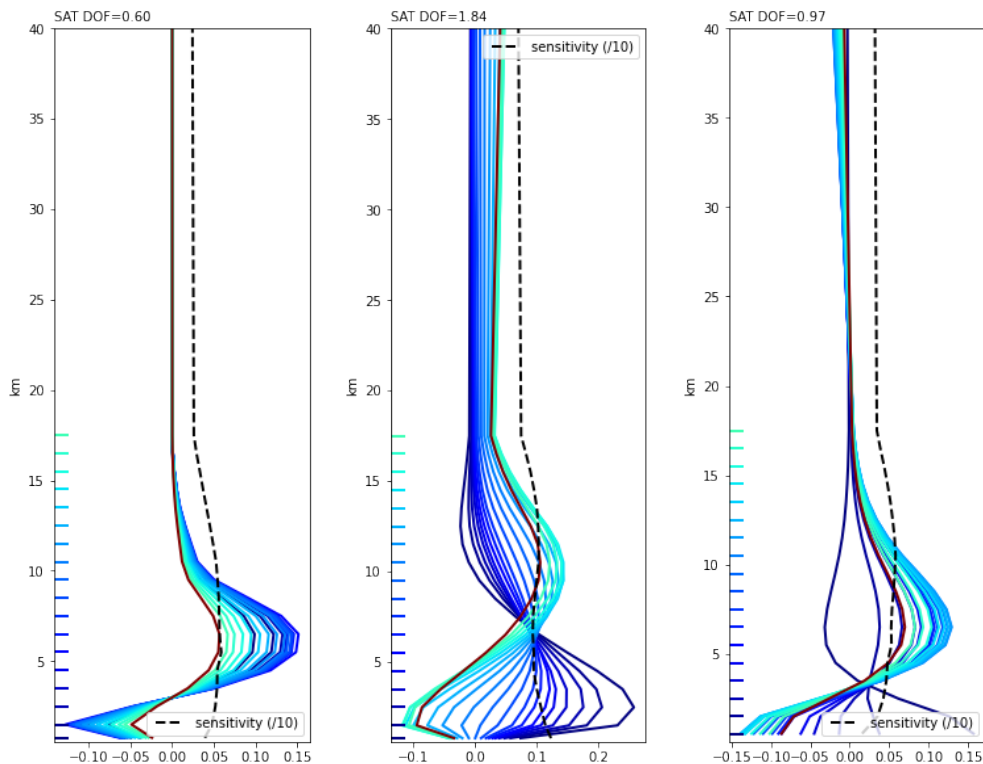


Figure 2.6 Typical averaging kernels for 3 IASI A pixels at (from left to right) Thule (Greenland), Garmisch (Germany) and Arrival Heights (Antarctic). The averaging kernels shown here act on profiles relative to the *a-priori*.

2.2. Comparison methodology

Each FTIR measurement is co-located to all IASI pixels within a time difference of 3 hours and within a distance of 50 km around the effective location of the FTIR measurement. This effective location is derived

from an effective altitude, which is in turn obtained as a weighted mean of the altitude using the CO partial column profile as weight. This effective altitude is projected along the line of sight of the FTIR measurement and can reach distances up to 50km for the high solar zenith measurements.

For each co-located pair consisting of a single FTIR and IASI measurement, a sequence of operations is performed aiming to reduce the influence in the comparison of the two *a priori* profiles used in the FTIR and IASI retrieval methods (Rodgers *et al.*, 2003). A first step consists of regriding the FTIR *a priori* and retrieved profiles to the IASI grid. Secondly, the regrided FTIR *a priori* is substituted in the IASI retrieval and the third and final step consists of using the smoothing equation by applying the IASI averaging kernel on the FTIR retrieved and regrided profile and using the FTIR *a priori* as a common prior. All these steps follow the methodology described in Rodgers *et al.* (2003).

Regridding is done such that the total CO mass is conserved (Langerock *et al.*, 2014) and possible vertical mismatches between the station surface and the satellite pixel surface are corrected by extending the regrided FTIR profiles by the extrapolated FTIR *a priori*. All profiles in the comparison are plotted for a single measurement pair in Figure 2.7.

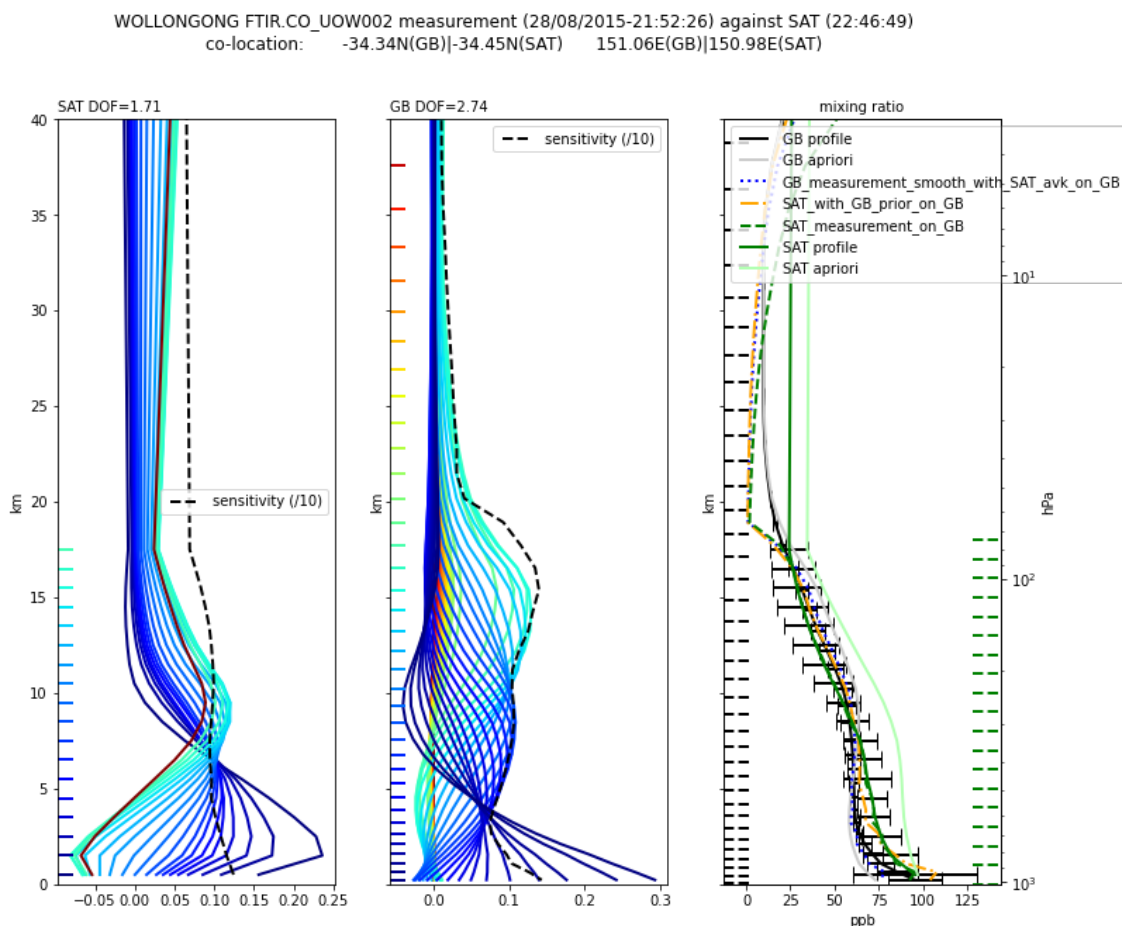


Figure 2.7 Detailed comparison plot for of a single IASI-A CO pixel (green profile in the right panel) against a co-located FTIR measurement (black profile). The right panel contains all profiles calculated for this comparison, the most left plot is the IASI AVK, the middle panel shows the FTIR AVK (all AVK act on VMR profiles relative to the *a priori*).

As mentioned in Section 2.1, the common prior is chosen to be the FTIR *a priori* profile because the IASI *a priori* profile shows an increased bias for the southern hemisphere. Here the comparison methodology deviates from the methodology described in the IASI CO NRT Validation Report [VR1], where the IASI *a priori* is chosen as a common prior. This choice does not affect the overall conclusions. Because the IASI prior is underestimating at Toronto, the substitution method introduces a positive bias. Toronto is therefore left out from the overall statistics table with the smoothed FTIR data (see Table 2.2).

From the IASI averaging kernels presented in Figure 2.6, the IASI retrievals at higher latitudes show reduced DOF during the spring months. The mosaic plot of profile differences for Thule in Figure 2.8 shows the effect of the smoothing operation: it removes the underestimation below 10km during the spring months.

As a final step, from all IASI pixels that co-locate to a single FTIR measurement the four closest pixels are averaged. Only FTIR measurements with at least two co-located IASI profiles are taken into account. This reduces the noise in the comparisons (the standard deviation of the relative differences is reduced with approximately 3% when compared to a co-location to the closest pixel).

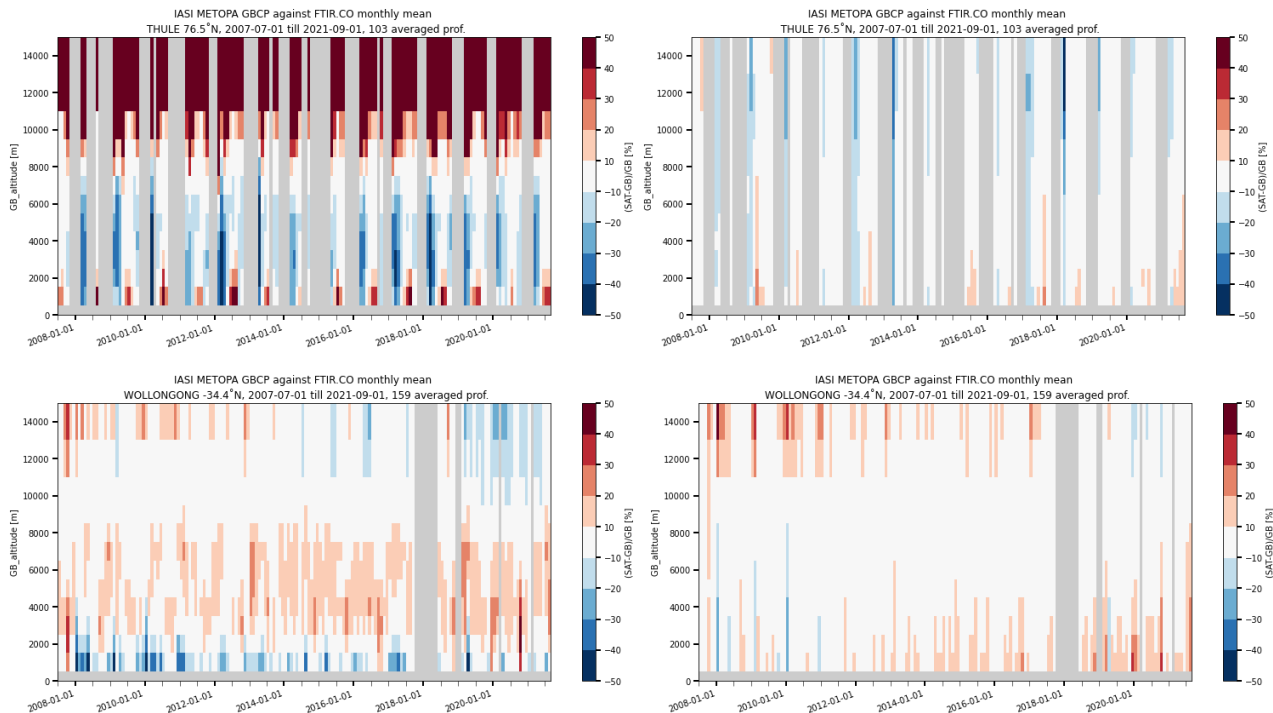


Figure 2.8 Mosaic plot of vertical profile differences at the high latitude station Thule (top row) and Wollongong (bottom row) for IASI-A to demonstrate the effect of the smoothing operation. The left plot shows the difference of the FTIR profile and the IASI profile regridded to the FTIR grid. The right panel shows the difference of the smoothed FTIR profile and the IASI profile (containing the FTIR *a priori*).

2.3. Comparison statistics.

Differences are calculated using either the FTIR NDACC data without any modification against the IASI columns calculated on the FTIR grid or using the smoothed FTIR columns against the IASI columns (containing the FTIR *a priori*). Table 2.1 and Table 2.2 provide the details per station for the relative differences and Pearson correlation coefficients for both the direct comparison and the comparison using the smoothed FTIR columns. Figure 2.9 and Figure 2.10 contain respectively a mosaic and histogram visualisation of the differences provided in the two tables.

The comparison data has the following characteristics:

1. Statistics for IASI-A and B are very similar.
2. The IASI prior at Toronto is too low and the prior alignment where the FTIR prior is substituted in the IASI profile introduces a systematic bias. The Toronto site is therefore left out from the statistics in Table 2.2.
3. A seasonal bias is observed in Figure 2.9, most strongly for the northern mid-latitudes and Arctic sites. This bias is related to the reduced sensitivity of the IASI retrieval. This is discussed in more detail in the next paragraph. From Table 2.1, Table 2.2 and Figure 2.10: most of the mid-latitude and tropical sites have biases within the optimal accuracy of 5% or only slightly exceed it with approx. 1.5pp. Paramaribo,

Porto Velho and Saint-Denis (Reunion) have higher biases, which is also observed in the comparison with MOPPIT (Fig7,8 in [VRL3]). The limited number of FTIR measurements and sites (some are mountain sites) makes it difficult to draw conclusions on the cause of this bias.

- The smoothed comparison shows higher biases for high latitude stations: this is related to the smoothing operation which takes into account the reduced IASI sensitivity and reduces the underestimation during local winter. Target accuracy for high latitude sites is 20% and the observed biases are below this value.

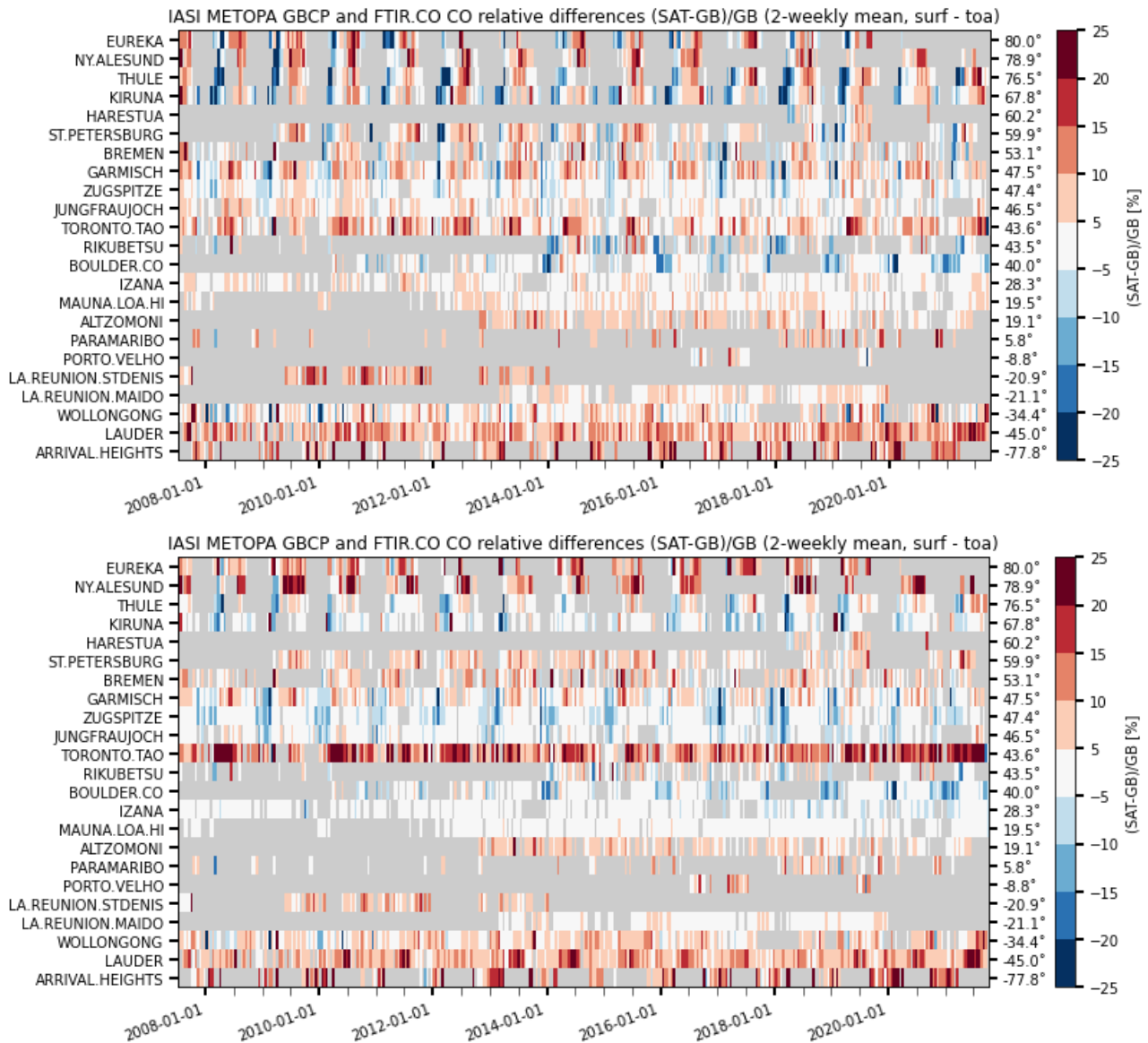


Figure 2.9 Mosaic of weekly mean relative differences for the direct comparison (top) and the comparison with prior alignment and smoothing (bottom). Smoothing reduces the seasonal dependence in the Arctic. Because the SAT prior at Toronto is underestimating, the prior alignment introduces a systematic bias.

Table 2.1. Statistics for the direct comparison between IASI Metop-A/B and FTIR CO total columns for the entire IASI CO CDR dataset (the column “std” is the standard deviation of the local FTIR columns relative to the standard deviation of the IASI columns, R is the Pearson correlation coefficient, rel. diff. is the mean of the relative differences IASI minus FTIR in percentage).

	Metop-A					Metop-B				
	# meas.	std.	R	rel. diff. %	std. rel. diff. %	# meas.	std.	R	rel. diff. %	std. rel. diff. %
EUREKA	5437	0.8	0.49	1.68	16.65	3235	0.7	0.56	1.06	16.41
NY.ALESUND	1087	1.1	0.69	4.9	11.62	510	1	0.71	4.99	10.37
THULE	7191	0.8	0.56	1.07	14.81	6033	0.8	0.63	1.81	14.26
KIRUNA	1957	1	0.56	-0.79	11.82	1506	1	0.54	0.08	11.71
HARESTUA	235	1.3	0.76	1.08	7.84	256	1.2	0.81	3.22	7.26
ST.PETERSBURG	3389	0.9	0.72	4.07	9.56	2339	0.9	0.75	4.49	8.75
BREMEN	989	0.9	0.77	1.95	9.71	744	0.8	0.69	3.08	11.08
GARMISCH	9360	0.9	0.76	4.89	9.95	5647	0.8	0.75	6.31	9.85
ZUGSPITZE	9990	1	0.86	0.21	6.8	5391	1	0.87	-0.21	6.31
JUNGFRAUJOCH	2456	1	0.9	2.99	5.51	1385	1	0.91	1.96	5.46
TORONTO.TAO	2381	0.8	0.82	7.72	9.7	1933	0.7	0.85	7.92	9.6
RIKUBETSU	187	0.7	0.79	-0.45	10.73	173	0.8	0.74	-0.21	11.03
BOULDER.CO	3736	0.9	0.86	-3	8.34	4082	0.9	0.86	-2.24	8.44
IZANA	2265	1	0.95	3.33	3.6	1869	1.1	0.95	3.23	3.54
MAUNA.LOA.HI	2510	1	0.97	3.65	4.17	2270	1	0.97	2.86	4.05
ALTZOMONI	1845	1	0.92	6.32	4.94	1698	1.1	0.9	5.7	5.12
PARAMARIBO	339	0.8	0.9	9.18	5.37	198	0.7	0.94	9.92	6.21
PORTO.VELHO	428	1	0.95	0.36	8.82	477	0.9	0.97	2.98	8.82
LA.REUNION.STDENIS	620	0.7	0.97	10.54	5.69	200	0.9	0.95	10.43	3.8
LA.REUNION.MAIDO	4796	1	0.98	4.28	3.69	4977	0.9	0.98	4.28	3.69
WOLLONGONG	9179	1	0.78	3.81	11.25	4716	0.9	0.83	4.69	10.61
LAUDER	3384	0.8	0.94	10.46	7.1	3388	0.8	0.94	10.1	7.03
ARRIVAL.HEIGHTS	748	0.7	0.78	13.15	15.05	699	0.8	0.8	13.44	13.4
Mean		0.92	0.81	3.97	8.81		0.9	0.82	4.34	8.56

Table 2.2. Statistics overview for the comparison with smoothing and prior alignment between IASI Metop-A/B and FTIR CO total columns for the entire IASI CO CDR dataset (table columns have similar meaning as in Table 2.1).

	Metop-A					Metop-B				
	# meas.	std.	R	rel. diff. %	std. rel. diff. %	# meas.	std.	R	rel. diff. %	std. rel. diff. %
EUREKA	5437	0.6	0.7	11.94	15.76	3235	0.6	0.8	11.66	14.23
NY.ALESUND	1087	1.1	0.76	10.96	11.19	510	1.1	0.82	9.68	9.86
THULE	7191	0.9	0.81	1.13	10.52	6033	0.8	0.83	1.72	10.37
KIRUNA	1957	1	0.76	-3.58	8.74	1506	1	0.77	-3.72	8.02
HARESTUA	235	1.2	0.83	3.88	6.41	256	1.1	0.86	5.95	6.31
ST.PETERSBURG	3389	0.9	0.87	5.92	6.8	2339	0.9	0.88	6.54	6.35
BREMEN	989	0.9	0.84	5.82	9.63	744	0.8	0.78	6.79	10.29
GARMISCH	9360	0.9	0.8	2.5	8.89	5647	0.9	0.78	3.85	9
ZUGSPITZE	9990	1	0.85	-3.75	6.5	5391	1	0.86	-4.17	6.06
JUNGFRAUJOCH	2456	0.9	0.89	-1.05	5.32	1385	0.9	0.9	-1.89	5.64
TORONTO.TAO	2381	0.8	0.8	15.09	11.45	1933	0.8	0.84	15.01	10.8
RIKUBETSU	187	0.8	0.89	1.42	8.13	173	0.9	0.84	2.4	8.71
BOULDER.CO	3736	0.9	0.88	-3.63	7.73	4082	0.9	0.86	-3.31	8.23
IZANA	2265	1	0.97	-2.81	2.69	1869	1	0.97	-2.73	2.55
MAUNA.LOA.HI	2510	0.9	0.98	0.42	3.08	2270	0.9	0.98	-0.25	3.21
ALTZOMONI	1845	1	0.92	6.31	4.81	1698	1	0.89	5.45	5.06
PARAMARIBO	339	0.9	0.9	5.93	5.19	198	0.8	0.94	7.01	5.41
PORTO.VELHO	428	0.9	0.96	6.35	8.86	477	0.8	0.97	8.87	8.75
LA.REUNION.STDENIS	620	0.8	0.97	7.1	4.86	200	1	0.95	7.62	3.96
LA.REUNION.MAIDO	4796	0.9	0.99	3.12	2.94	4977	0.9	0.99	3.24	3.04
WOLLONGONG	9179	0.9	0.88	5.39	8.78	4716	0.8	0.92	6.38	8.24
LAUDER	3384	0.9	0.95	9.49	7.36	3388	0.9	0.89	8.67	7.57
ARRIVAL.HEIGHTS	748	1	0.83	12.61	12.49	699	1	0.87	12.44	9.7
Mean		0.92	0.87	3.89	7.58		0.91	0.88	4.19	7.30

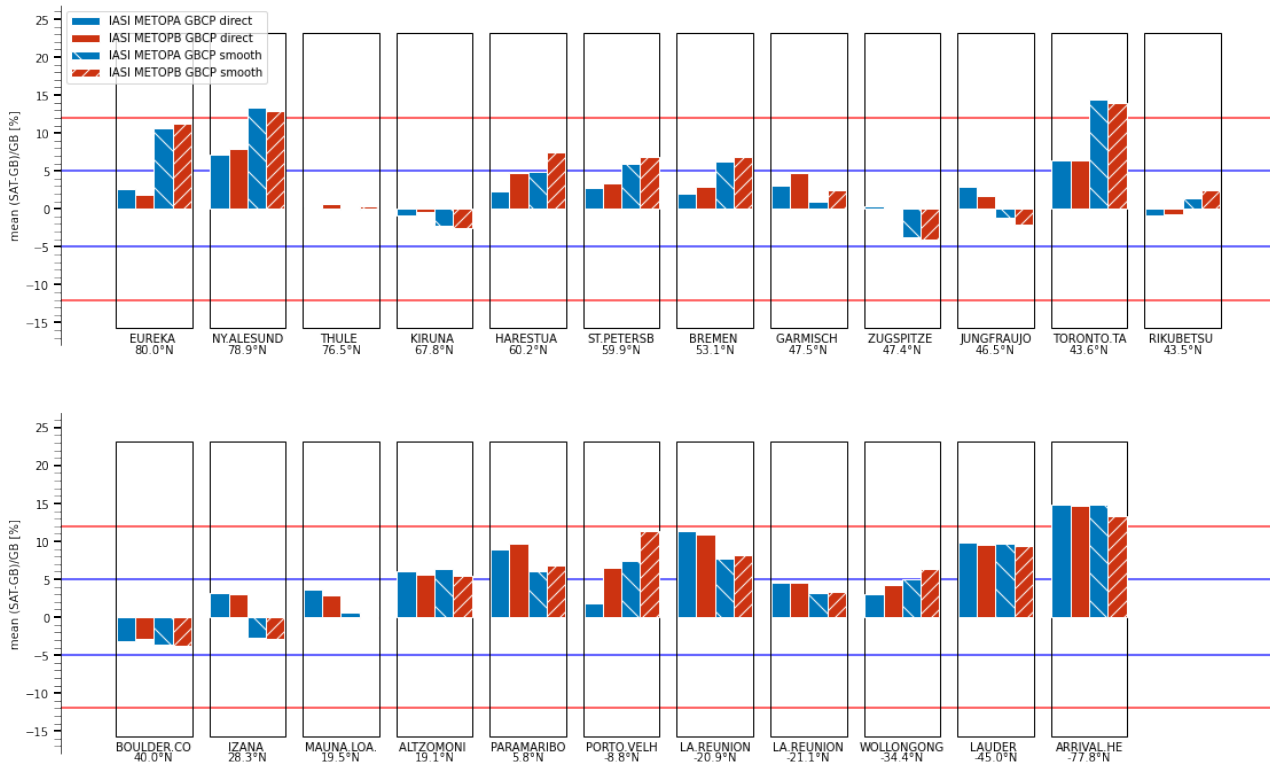


Figure 2.10 Histogram plot of the relative biases in Tables 2.1 and 2.2. The horizontal blue lines show the optimal accuracy (5%), red horizontal lines show the target uncertainties (12%), valid for mid-latitudes and tropical stations.

2.4. Long term stability of comparison results

To estimate trends in the relative differences, we have applied a least squares fitting of a first order polynomial combined with a third order annual periodic function through the time series of weekly median relative differences². Although the observed trends in atmospheric CO depend on regions and changes in local emissions (Zheng 2019), we regrouped all data in latitude bins in order to reduce the gaps in the time series. This can be justified by mentioning that no NDACC site falls in the regions with positive trends in atmospheric CO (Zheng 2019).

Trend estimates are considered significant if the p-value is below 0.1, which is why the Arctic and Antarctic region are not discussed here. For the northern mid-latitude sites (30°;60°N) a negative trend is observed of the order -0.33%/y (+-0.07%/y) in IASI A and -0.30%/y (+-0.12%/y) for IASI B (Figure 2.11 and Table 2.3). In the smoothed comparison (table not included), these trends are slightly reduced with approximately 0.1%/y. A similar negative trend is observed in the tropics (Figure 2.12 and Table 2.3). For the southern mid latitudes (30°;60°S) the observed trends are +0.40%/y (+-0.08%/y) for IASI A and +0.51%/y (+-0.13%/y) for IASI B (Figure 2.13 and Table 2.3). It should be mentioned that the southern mid-latitudes bin only contains two sites: Wollongong (Australia) and Lauder (New Zealand).

A possible cause for the observed trends could be related to the use of a constant prior for the IASI (constant both in time and location) and the NDACC retrievals (constant in time) in combination with the different sensitivities of both retrievals. Using a constant prior in combination with a negative trend in the atmospheric CO will generate a changing systematic smoothing error in the retrieval. For the northern hemisphere where the IASI prior is generally underestimating (Figure 2.4), the systematic smoothing error will decrease while for the southern hemisphere the systematic smoothing error will increase as the IASI prior is overestimating.

²Curve fitting as described in <https://gml.noaa.gov/ccgg/mbl/crvfit/crvfit.html>

The different sensitivities for IASI and NDACC in the retrieval will generate different smoothing errors and can explain the observed trends in the differences.

The seasonal amplitude is estimated at approximately $\pm 8\%$ for the northern mid-latitudes and remains within the target product accuracy (12% with an optimal value of 5%). The amplitude at the Arctic reaches 14% and also lies within the target accuracy (20% for low signal situations, with optimal value of 10%). The seasonal cycle is below 3% for the tropical sites and the southern mid-latitudes. Only one site provides data in Antarctica and this could explain the high amplitude estimate ($>50\%$).

Figure 2.14 shows the solar zenith angle dependence of the seasonal bias for a rolling mean time series of the relative differences for the direct comparison (the use of the rolling means reduces the impact of high pollution events). All biases remain below the threshold uncertainty of 25%. For some months in some years, the target product accuracy for this rolling mean is exceeded: eg local winter months in the southern mid-latitudes with high SZA. In similar plots for the smoothed comparison in Figure 2.15 the seasonal dependence is reduced.

Table 2.3. Trend and annual cycle (amplitude) estimates for the time series of relative differences in the different latitudinal bins for the direct comparison (* $p < 0.1$, ** $p < 0.05$, and * $p < 0.01$). The standard error of the trend estimate (one sigma) is provided. Estimates for the amplitude at the Arctic and Antarctica should be treated with care because of gaps during local winter months.**

	Metop-A			Metop-B		
	Trend [%/y]	Trend std [%/y]	Amplitude [%/y]	Trend [%/y]	Trend std [%/y]	Amplitude [%/y]
Arctic	-0.04	0.10	14.62***	0.02	0.19	14.06***
NH mid-latitudes	-0.33***	0.07	8.91***	-0.29**	0.12	7.86***
Tropics	-0.30***	0.07	1.17**	-0.36***	0.08	0.54
SH mid-latitudes	0.40***	0.08	2.82***	0.51***	0.13	2.06**
Antarctica	0.22	0.20	51.84***	-0.4	0.45	136.17***

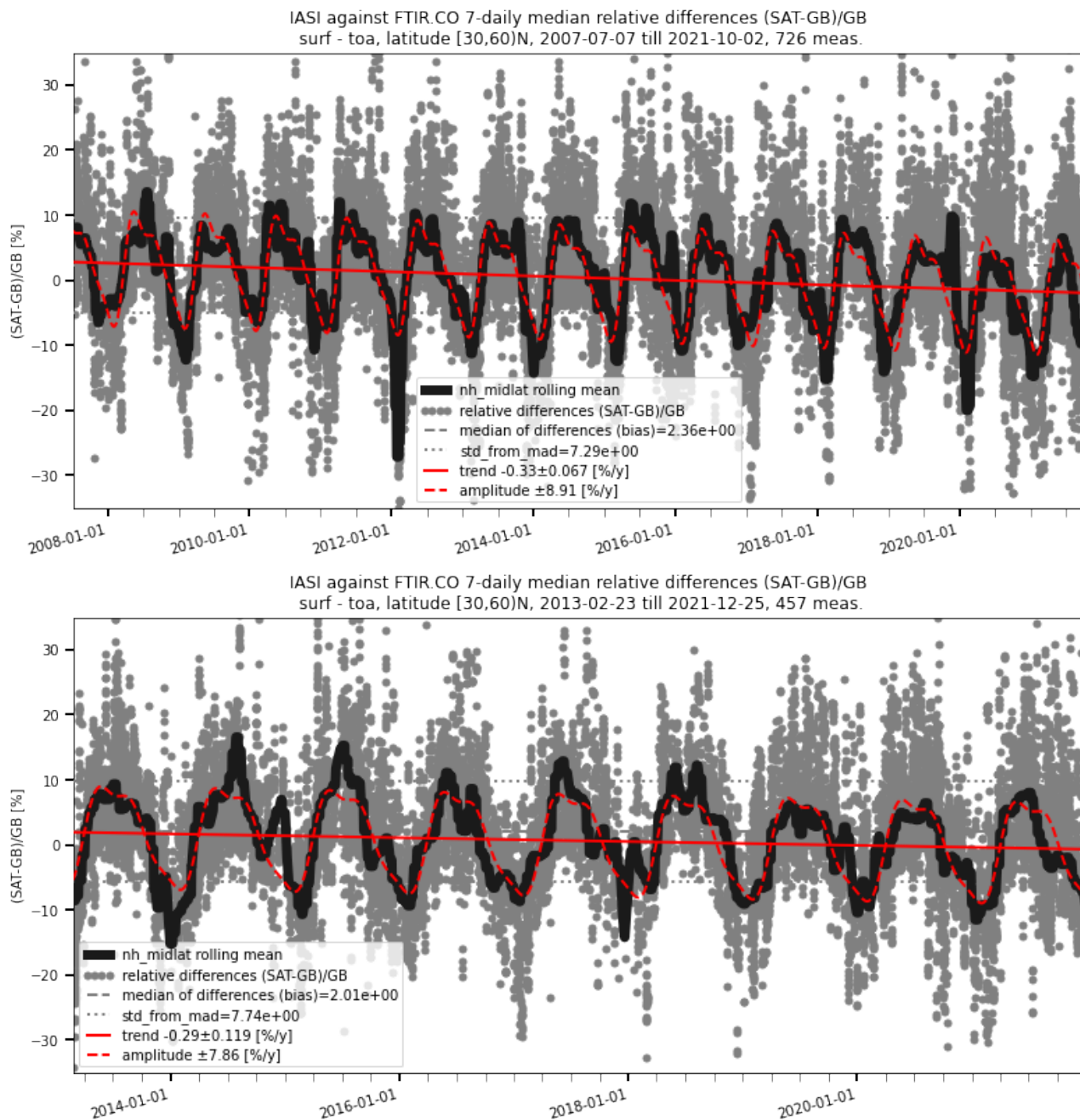


Figure 2.11 Trend analysis for the northern hemisphere NDACC sites. The black line is the rolling mean through the individual relative differences (grey circles). The least square fitting (red) is obtained on the weekly median values. Top is IASI-A, bottom is IASI-B.

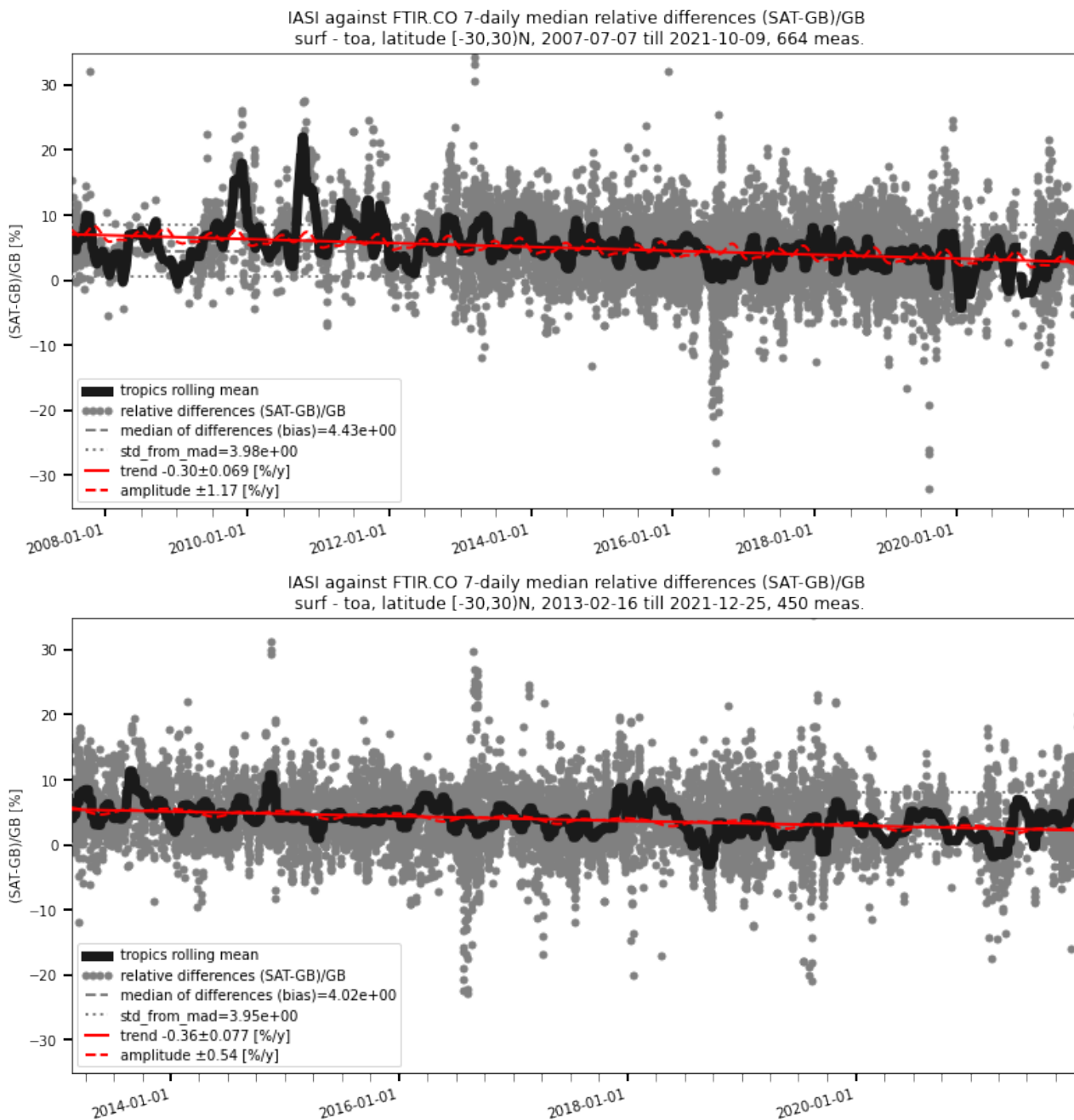


Figure 2.12 Trend analysis for the tropical NDACC sites. The black line is the rolling mean through the individual relative differences (grey circles). The least square fitting (red) is obtained on the weekly median values. Top is IASI-A, bottom is IASI-B.

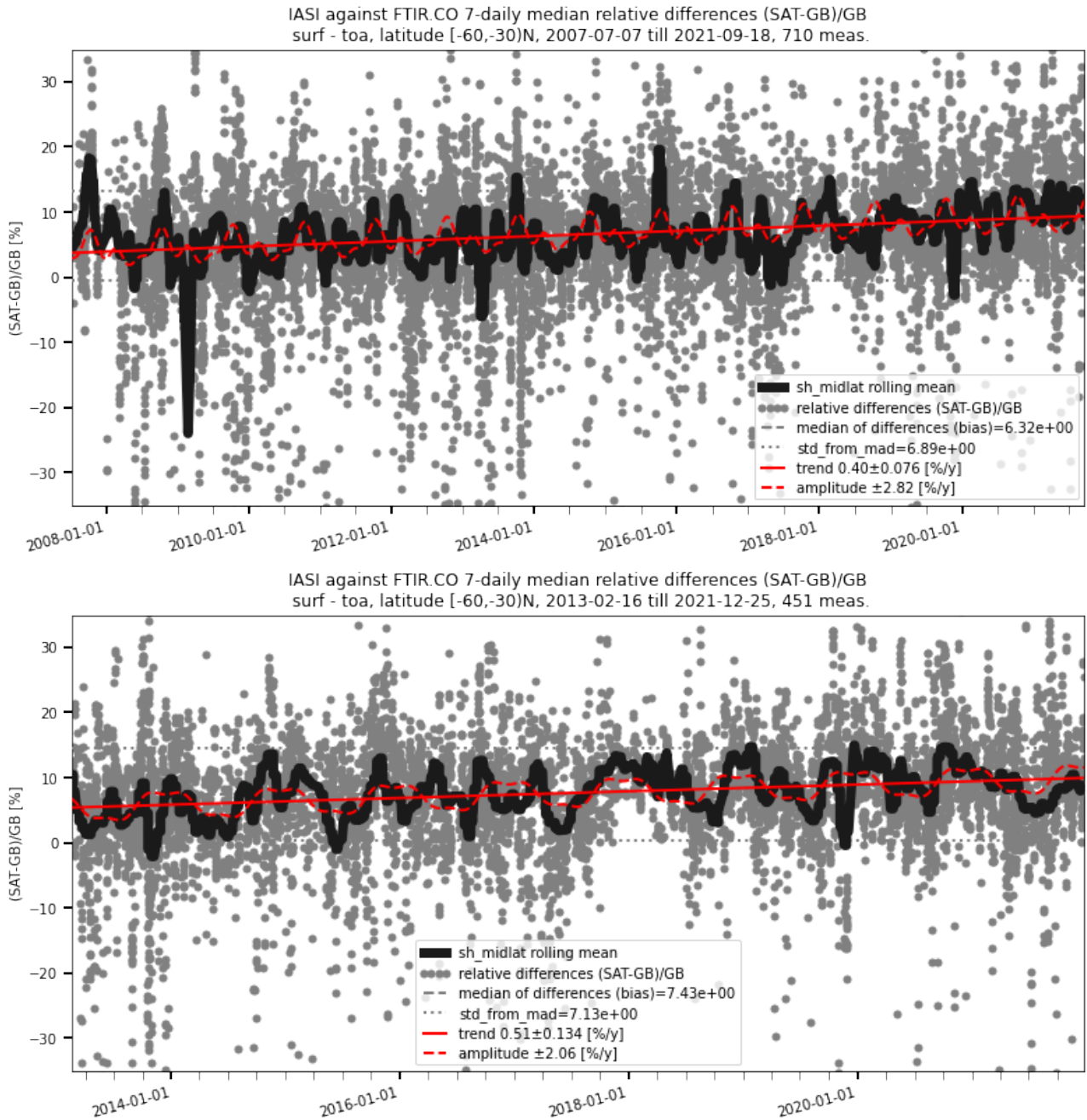


Figure 2.13 Trend analysis for the southern hemisphere NDACC sites. The black line is the rolling mean through the individual relative differences (grey circles). The least square fitting (red) is obtained on the weekly median values. Top is IASI-A, bottom is IASI-B.

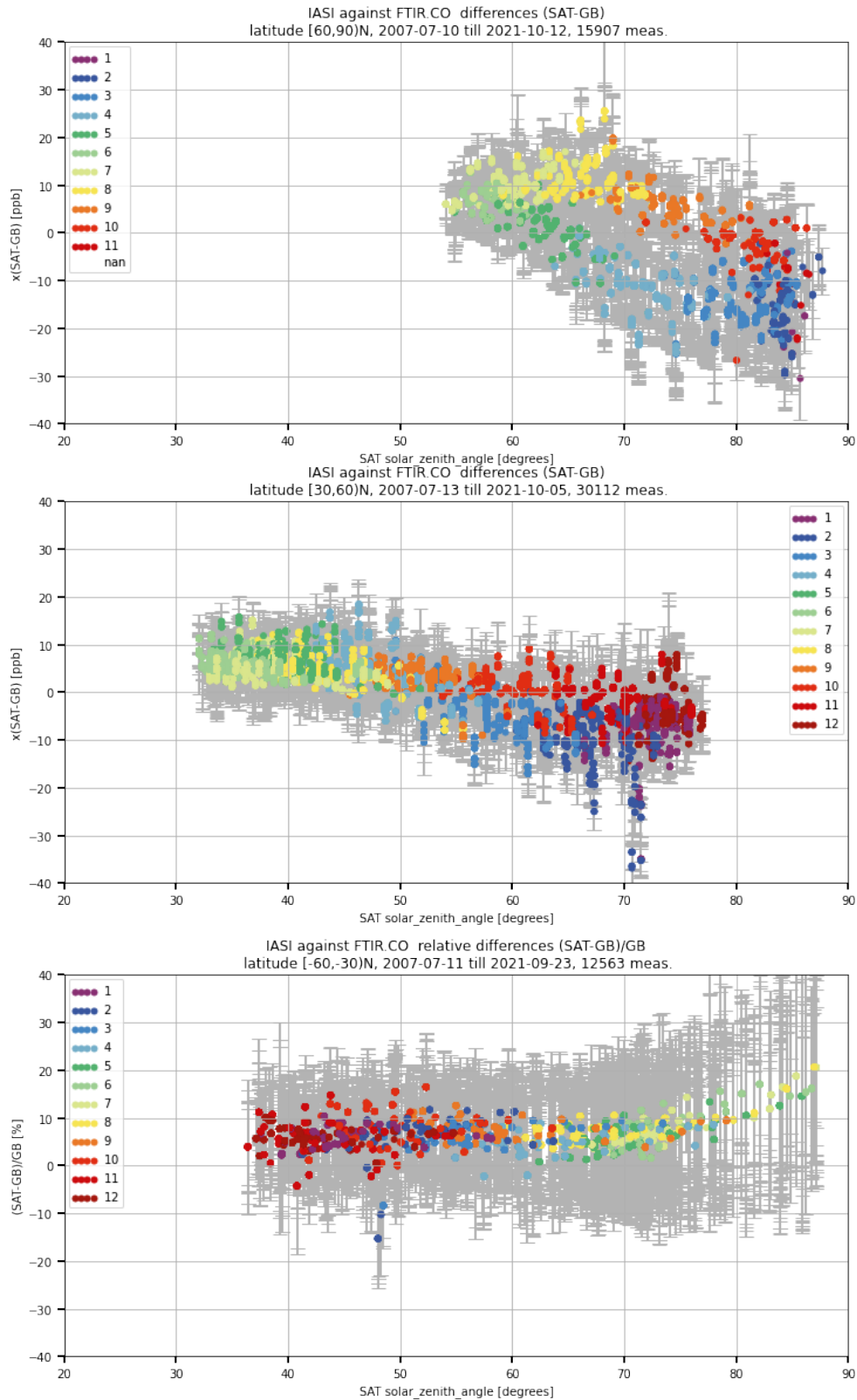


Figure 2.14 IASI A Direct comparison: bias vs the IASI solar zenith angle, colored according to month of the year. A clear seasonal cycle appears for the Arctic sites (+15%) and the northern mid-latitude sites (+9%). To reduce scatter and the effect of high pollution (fire) events, a rolling mean through daily means is used in these plots.

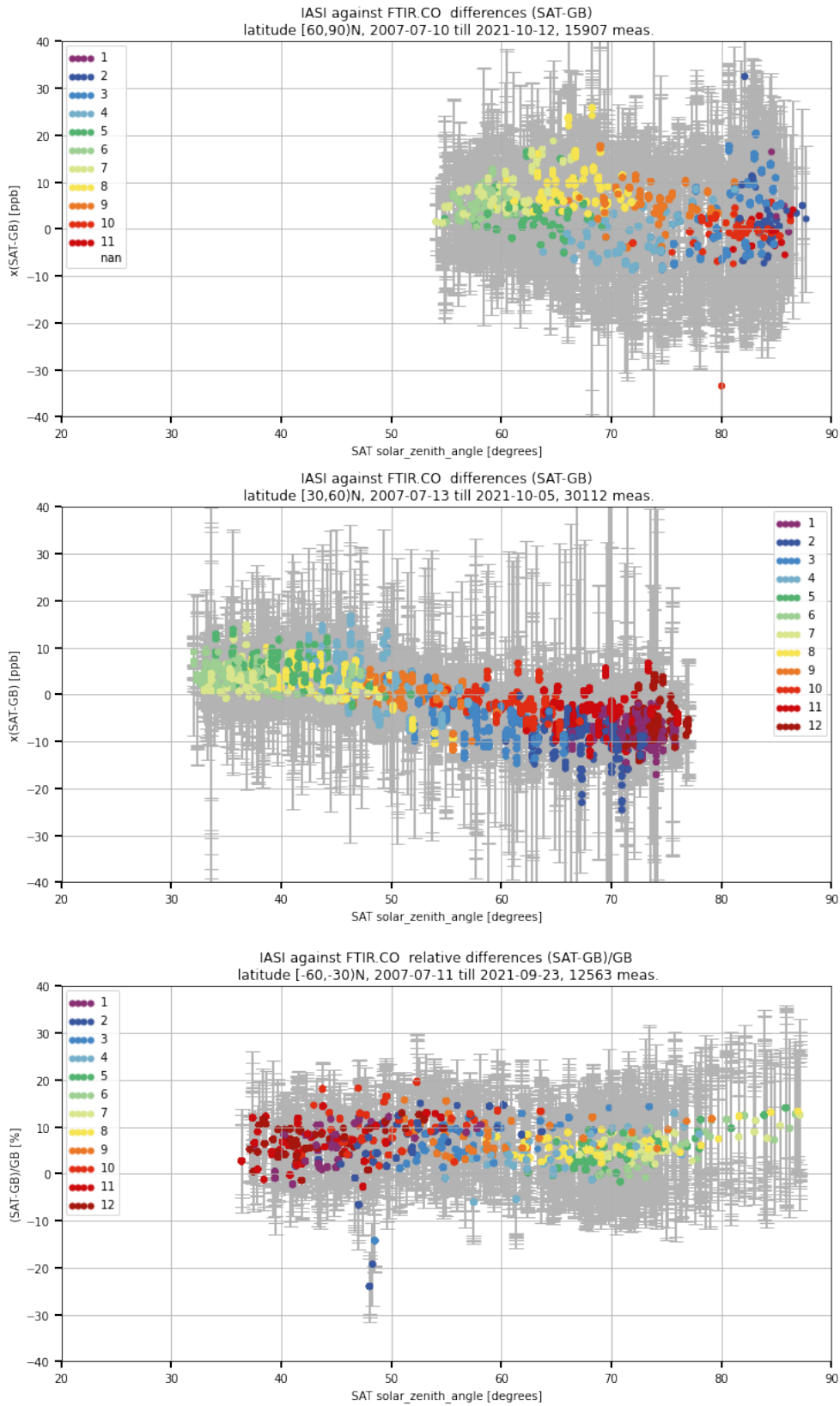


Figure 2.15 IASI A Smoothed-enabled comparison: similar as in Figure 3.1, bias vs the IASI solar zenith angle, coloured according to month of the year. The seasonal cycle is reduced: for the Arctic sites and the northern mid-latitude sites (+-8%).

3. DISCUSSION AND CONCLUSIONS

Accuracy. From Table 2.2, we see that the relative differences (for the comparison with the smoothed columns) are ranging between -3.75 for Zugspitze to 12.49% for Arrival Heights. Out of the 17 stations (excluding high latitude stations and Toronto) considered in this smoothed comparison, biases for 15 stations are below 6.5%: e.g. at Bremen the bias is 5.82% with a standard deviation of 9.63, for Garmisch 2.5 % [8.89], for Boulder -3.63% [7.73] or for Izana -2.81% [2.69]. The estimated bias for all stations but one is below the product required target accuracy of 12% [AD2] for both the IASI A and IASI B CDRs. Only the Antarctic site at Arrival Heights (77.5°S of latitude) exceeds the target accuracy slightly with 0.6pp (smoothing comparison). A similar remark holds for the direct comparison statistics in Table 2.1 but some care must be taken because to the seasonal cycle in the Northern Hemisphere produces lower biases in Table 2.1.

Correlation. From the statistics Tables 2.1 and 2.2 we learn that the comparison of the smoothed columns improves the overall correlation with 0.06: from 0.81 to 0.87 for IASI A.

Uncertainty. When comparing the mean differences in Table 2.1 and 2.2 against the reported measurement systematic uncertainty, the mean of the differences (being approx.. 4%) is smaller or of the same order as the reported FTIR systematic uncertainty. The overall mean relative positive bias does not change much between the direct and smoothing enabled comparison method, but the standard deviation on the relative differences is reduced with more than 1pp in the smoothing setup, to a value of approximately 7%. For a comparison setup where no pixels are averaged and only the closest FTIR-IASI pair is considered, the standard deviation on the differences is 10%. The latter should be compared against the combined random uncertainty of the two measurements FTIR and IASI. Since IASI only reports a total uncertainty, no conclusion can be made on the random uncertainty. However, the order of magnitude of the IASI uncertainty and its latitudinal dependence seems to give a realistic value when considering the comparison statistics in Tables 2.1 and 2.2.

Seasonal dependence. The IASI data contains a seasonal dependence and underestimates the CO column in the spring months for high latitude stations and northern mid-latitude stations (+8%) and is negligible for the tropics and southern mid-latitudes. The seasonal dependence does not exceed the threshold accuracy. Although the amplitude is below the target accuracy of 12%, this target of 12% is not always met when looking at the biases during certain months. The seasonal dependence is significantly reduced in the smoothing-enabled comparison in Figure 2.15. For the southern mid-latitudes the local winter months measure with higher solar zenith angle and the relative differences show a clear dependency on the $SZA > 75^\circ$ reaching values above the threshold of 12% (but below the threshold accuracy 25%).

Trend in differences. For the northern mid-latitude sites (30°;60°N) a negative trend is observed of the order -0.33%/y (+0.07%/y) in IASI A and -0.30%/y (+0.12%/y) for IASI B (Figure 2.11). In the smoothed comparison, these trends are slightly reduced with approximately 0.1%/y. A similar negative trend is observed in the tropics. For the southern mid latitudes (30°;60°S) the observed trends are +0.40%/y (+0.08%/y) for IASI A and +0.51%/y (+0.13%/y) for IASI B (Figure 2.13). The sign change in the trend from northern to southern hemisphere is attributed to a changing smoothing error in the IASI retrievals (decreasing in the NH and increasing in the SH) caused by the changing CO atmospheric content.

General Conclusion. The IASI CO climate data records for IASI A and B perform very similar and meet the target requirements on accuracy. Excluding high latitude stations, then 15 out of 17 stations have relative biases estimated below 6.5% which is close to the optimal accuracy of 5% and well below the target accuracy of 12%. The target accuracy can be exceeded during local winter months with high solar zenith angle measurements but exceedances remain below the threshold accuracy of 25%. For high latitude sites the biases fall within the (enlarged) target accuracy of 20%. A seasonal cycle is observed at high latitude stations, but also in the northern mid-latitudes where the amplitude is estimated at approximately +8%/y for both IASI A and B. A negative trend in the relative differences of approx. -0.3%/y appears in the northern mid-latitudes and tropics. For the southern mid-latitudes a positive trend of approx.. +0.4%/y is observed.

4. ACKNOWLEDGMENTS

The data used in this publication were obtained as part of the Network for the Detection of Atmospheric Composition Change ([NDACC](#)) and are publicly available. The author would like to thank Minqiang Zhou for interesting discussions. Rosa Astoreca and Maya George made valuable suggestions for improving the contents of the report.

The measurements in Paramaribo have been supported by the BMBF (German Ministry of Research and Education) in the project ROMIC-II subproject TroStra (01LG1904A) and by the AWI Bremerhaven. The AWI Bremerhaven also supported the measurements in Ny Alesund. We also thank the Senate of Bremen for financial support.

The multi-decadal monitoring program of ULiege at the Jungfraujoch station has been primarily supported by the F.R.S.-FNRS and BELSPO (both in Brussels, Belgium) and by the GAW-CH programme of MeteoSwiss. The International Foundation High Altitude Research Stations Jungfraujoch and Gornergrat (HFSJG, Bern) supported the facilities needed to perform the FTIR observations.

FTIR measurements in Mexico are supported by Dr. Alejandro Bezanilla and partly financed by UNAM with grant DGAPA-PAPIIT IN111521.

The NDACC stations Bremen, Garmisch, Izaña, Kiruna, Ny-Ålesund, Paramaribo and Zugspitze have been supported by the German Bundesministerium für Wirtschaft und Energie (BMWi) via DLR under grants 50EE1711A, B and D.

5. REFERENCES

5.1. Applicable documents

[AD1] FORLI-CO Product Specification, Requirement And Assessment SAF/O3M/ULB/FORLICO_PSRA Issue 1, 21/01/2015

[AD2] Product Requirements Document SAF/AC/FMI/RQ/PRD/001 Issue 1.9.1, 03/02/2022

[PUM] **Product User Manuel, SAF/AC/ULB/PUM/004, Issue 1.1, 27/04/2021.**

[VR1] NRT IASI CO Validation Report SAF/O3M/LATMOS/VR/001 Issue 1.9.1, 17/11/2015

[VRL3] IASI CO L3 Validation report SAF/AC/LATMOS/VR/IASI_CO_L3, issue 10/2023, 16/10/2023.

5.2. Reference documents

Hilton, F.; August, T.; Barnet, C.; Bouchard, A.; Camy-Peyret, C.; Clarisse, L.; Clerbaux, C.; Coheur, P.-F.; Collard, A.; Crevoisier, C.; Dufour, G.; Edwards, D.; Faijan, F.; Fourrié, N.; Gambacorta, A.; Gauguin, S.; Guidard, V.; Hurtmans, D.; Illingworth, S.; Jacquinet-Husson, N.; Kerzenmacher, T.; Klaes, D.; Lavanant, L.; Masiello, G.; Matricardi, M.; McNally, T.; Newman, S.; Pavelin, E.; Péquignot, E.; Phulpin, T.; Remedios, J.; Schlüssel, P.; Serio, C.; Strow, L.; Taylor, J.; Tobin, D.; Uspensky, A. & Zhou, D. Hyperspectral Earth Observation with IASI. *Bull. Am. Meteorol. Soc.*, 93(3), 347-370, doi: 10.1175/BAMS-D-11-00027.1, 2012.

Clerbaux, C.; Boynard, A.; Clarisse, L.; George, M.; Hadji-Lazaro, J.; Herbin, H.; Hurtmans, D.; Pommier, M.; Razavi, A.; Turquety, S.; Wespes, C. & Coheur, P. F. Monitoring of atmospheric composition using the thermal infrared IASI/MetOp sounder. *Atmos. Chem. Phys.*, 9(16):6041-6054, 2009

De Wachter, E., Barret, B., Le Flochmoën, E., Pavelin, E., Matricardi, M., Clerbaux, C., Hadji-Lazaro, J., George, M., Hurtmans, D., Coheur, P.-F., Nedelec, P., and Cammas, J. P.: Retrieval of MetOp-A/IASI CO profiles and validation with MOZAIC data, *Atmos. Meas. Tech.*, 5, 2843–2857, <https://doi.org/10.5194/amt-5-2843-2012>, 2012

George, M., Clerbaux, C., Bouarar, I., Coheur, P.-F., Deeter, M. N., Edwards, D. P., Francis, G., Gille, J. C., Hadji-Lazaro, J., Hurtmans, D., Inness, A., Mao, D., and Worden, H. M.: An examination of the long-term CO records from MOPITT and IASI: comparison of retrieval methodology, *Atmos. Meas. Tech.*, 8, 4313–4328, <https://doi.org/10.5194/amt-8-4313-2015>, 2015

Hurtmans, D.; Coheur, P.; Wespes, C.; Clarisse, L.; Scharf, O.; Clerbaux, C.; Hadji-Lazaro, J.; George, M. & Turquety, S. FORLI radiative transfer and retrieval code for IASI. *J. Quant. Spectrosc. Radiat. Transfer*, 113, 1391-1408, 2012.

Langerock, B., De Mazière, M., Hendrick, F., Vigouroux, C., Desmet, F., Dils, B., and Niemeijer, S.: Description of algorithms for co-locating and comparing gridded model data with remote-sensing observations, *Geosci. Model Dev.*, 8, 911–921, <https://doi.org/10.5194/gmd-8-911-2015>, 2015

Rodgers, C. D. *Inverse methods for atmospheric sounding: Theory and Practice*, Series on Atmospheric, Oceanic and Planetary Physics - Vol. 2. World Scientific, Singapore, New Jersey, London, Hong Kong, 2000

Rodgers, C. D. and Connor, B. J.: Intercomparison of remote sounding instruments, *J. Geophys. Res.*, 108, 4116, doi:10.1029/2002JD002299, 2003.

Vigouroux, C., De Mazière, M., Errera, Q., Chabrilat, S., Mahieu, E., Duchatelet, P., Wood, S., Smale, D., Mikuteit, S., Blumenstock, T., Hase, F., and Jones, N.: Comparisons between ground-based FTIR and

MIPAS N₂O and HNO₃ profiles before and after assimilation in BASCOE, *Atmos. Chem. Phys.*, 7, 377–396, doi:10.5194/acp-7-377-2007, 2007

Vigouroux, C., Langerock, B., Bauer Aquino, C. A., Blumenstock, T., Cheng, Z., De Mazière, M., De Smedt, I., Grutter, M., Hannigan, J. W., Jones, N., Kivi, R., Loyola, D., Lutsch, E., Mahieu, E., Makarova, M., Metzger, J.-M., Morino, I., Murata, I., Nagahama, T., Notholt, J., Ortega, I., Palm, M., Pinardi, G., Röhling, A., Smale, D., Stremme, W., Strong, K., Sussmann, R., Té, Y., van Roozendaal, M., Wang, P., and Winkler, H.: TROPOMI–Sentinel-5 Precursor formaldehyde validation using an extensive network of ground-based Fourier-transform infrared stations, *Atmos. Meas. Tech.*, 13, 3751–3767, <https://doi.org/10.5194/amt-13-3751-2020>, 2020

Wespes, C., Hurtmans, D., Clerbaux, C., Santee, M. L., Martin, R. V., and Coheur, P. F.: Global distributions of nitric acid from IASI/MetOP measurements, *Atmos. Chem. Phys.*, 9, 7949–7962, doi:10.5194/acp-9-7949-2009, 2009

Zheng, B., Chevallier, F., Yin, Y., Ciais, P., Fortems-Cheiney, A., Deeter, M. N., Parker, R. J., Wang, Y., Worden, H. M., and Zhao, Y.: Global atmospheric carbon monoxide budget 2000–2017 inferred from multi-species atmospheric inversions, *Earth Syst. Sci. Data*, 11, 1411–1436, <https://doi.org/10.5194/essd-11-1411-2019>, 2019